BIOLOGICAL SCIENCES: Molecular Biology

Characterization of *N*-glycosylation and its Functional Role in SIDT1-Mediated RNA Uptake

Tingting Yang[1]*, Haonan Xiao[1]*, Xiulan Chen[2,6]*, Le Zheng[1], Hangtian Guo[1], Jiaqi Wang[1], Xiaohong Jiang[1], Chen-Yu Zhang[1,4]†, Fuquan Yang[2,6]†, Xiaoyun Ji[1,3,4,5]†

[1]The State Key Laboratory of Pharmaceutical Biotechnology, School of Life Sciences, Nanjing University, Nanjing, Jiangsu 210023, People's Republic of China.
[2]Key Laboratory of Protein and Peptide Pharmaceuticals & Laboratory of Proteomics, Institute of Biophysics, Chinese Academy of Sciences, Beijing 100101, China.
[3]Chemistry and Biomedicine Innovation Center (ChemBIC), Nanjing University, Nanjing, Jiangsu 210023, People's Republic of China.
[4]Institute of Artificial Intelligence Biomedicine, Nanjing University, Nanjing, Jiangsu 210023, People's Republic of China.
[5]Engineering Research Center of Protein and Peptide Medicine, Ministry of Education, China.
[6]University of Chinese Academy of Sciences, Beijing 100149, China.

* These authors contributed equally to this work.

To whom correspondence should be addressed. E-mail: xiaoyun.ji@nju.edu.cn (X.J.), fqyang@ibp.ac.cn (F.Y.), cyzhang@nju.edu.cn (C.Z.)

Running title:
Effect of SIDT1 *N*-glycosylation on RNA transport

Key words:
SIDT1, SIDT2, mammalian SID-1 transmembrane family, *N*-glycosylation, RNA transport, protein stability, intracellular localization of proteins

42 text pages, 5 figures

169 words in the abstract and 4528 words in the main text

Abstract

The mammalian SID-1 transmembrane family members, SIDT1 and SIDT2, are multi-pass transmembrane proteins that mediate the cellular uptake and intracellular trafficking of nucleic acids, playing important roles in the immune response and tumorigenesis. Previous work has suggested that human SIDT1 and SIDT2 are *N*-glycosylated, but the precise site-specific *N*-glycosylation information and its functional contribution remain unclear. In this study, we employ high-resolution liquid chromatography tandem mass spectrometry to comprehensively map the *N*-glycosites and quantify the *N*-glycosylation profiles of SIDT1 and SIDT2. Our results provide crucial information about the functional impact of *N*-glycosylation on SIDT1. In particular, removal of the *N*-glycosylation from SIDT1 results in a severe defect in RNA uptake. Further molecular mechanistic probing elucidates the essential role of *N*-linked glycans in regulating RNA binding, cell surface expression and protein stability of SIDT1. Our results reveal a potential functional role for *N*-glycosylation in the regulation of SIDT1-mediated RNA uptake and provide insights into the molecular mechanisms of this promising nucleic acid delivery system, with potential implications for therapeutic applications.

/body

INTRODUCTION

Mammalian SID-1 transmembrane family member 1 (SIDT1) and member 2 (SIDT2) are the human orthologs of *Caenorhabditis elegans* systemic RNA interference defective protein 1 (SID-1), which is required for transporting exogenous double-stranded RNA (dsRNA) into the cytoplasm and is therefore essential for systemic RNA interference in *Caenorhabditis elegans*[1-4]. Previous studies on SIDT1 and SIDT2 have implicated them in various biological processes such as glucose and lipid metabolism, immune response, and tumorigenesis, including breast, lung, gastrointestinal, pancreatic and non-small cell lung cancers (NSCLC), but the specific mechanisms are unknown[5-13]. In contrast, the role of SIDT1 and SIDT2 in regulating various physiological processes by mediating cellular RNA uptake and intracellular trafficking have been extensively studied, providing significant insights into their functional contributions.

SIDT1 mediates the internalization of extracellular microRNA (miRNA) and small interfering RNA (siRNA) and subsequent gene silencing, which has great therapeutic potential for a wide range of human diseases, such as cancer, viral infections, and cardiovascular diseases[14-18]. Similarly, SIDT2 mediates gymnosis, facilitating the uptake of naked single-stranded oligonucleotides into living cells[19]. In addition to being involved in extracellular RNA uptake, both SIDT1 and SIDT2 exhibit lysosomal membrane localization and play a crucial role in the activation of the innate immune response by transporting internalized dsRNA across the lysosomal membrane to engage the cytoplasmic retinoic acid-inducible gene I (RIG-I)-like receptors (RLRs) and thereby induce type I interferon (IFN-I) production[12,13,20]. SIDT2 also mediates the delivery of cellular DNA and RNA into lysosomes for degradation through an arginine-rich motif that

binds to RNA/DNA[21,22]. However, the precise link between the physiological processes associated with SIDT1 and SIDT2 and their critical role in nucleic acid transport activities remains unclear.

Sequence alignment and structure-based prediction indicate that most members of the mammalian SID-1 transmembrane family are multi-pass membrane proteins consisting of eleven transmembrane helices (TMs) and a large N-terminal extracellular domain (ECD). The ECD contributes to SIDT1- and SIDT2-dependent RNA transport and their direct binding to RNA[23]. In addition to RNA binding, previous studies have suggested that human SIDT1 and SIDT2 are *N*-glycosylated[24,25]. Glycosylation is the most abundant and diverse form of post-translational modification of proteins, and more than half of mammalian proteins are glycosylated[26]. Numerous roles have been ascribed to protein *N*-glycosylation[27]. In particular, *N*-glycans can intrinsically modulate protein folding and stability, provide protection against proteases, and mediate protein-ligand interactions. Proper protein *N*-glycosylation is also crucial for the formation of protein complexes, the modulation of protein-protein interactions and the correct assembly of higher order protein structures[28-31].

The mammalian SID-1 transmembrane family-dependent nucleic acid transport has been demonstrated in several *in vitro* and *in vivo* systems[12,13,15,17-19,21,22]. However, a clear understanding of the role of its *N*-glycosylation in this process has not been achieved. Further sequence analysis revealed that the *N*-glycosylation of SID1 transmembrane family members is conserved across mammals (Supplementary Fig. 1). The high conservation of *N*-glycosylation argues for an essential biological function, and it seems reasonable to assume that *N*-glycosylation plays an essential role in the mammalian SID-1

transmembrane family. We hypothesized that *N*-glycosylation of the mammalian SID-1 transmembrane family has important implications for RNA transport, RNA binding, protein stability, etc.

Here we report the first systematic characterization of site-specific *N*-glycosylation and the corresponding *N*-glycans of human SIDT1 and SIDT2 using high-resolution liquid chromatography-tandem mass spectrometry (LC-MS/MS). Through mutagenesis studies, we found that non-*N*-glycosylated SIDT1 is defective in RNA uptake. Furthermore, reduced *N*-glycosylation affects the RNA binding and protein stability of SIDT1. We found that SIDT1 relies on its *N*-glycosylation to achieve its correct functional localization. In the absence of *N*-glycosylation, SIDT1 is misfolded and largely retained within the endoplasmic reticulum (ER), leading to ER stress and preventing efficient translocation to the plasma membrane. Taken together, these observations unravel the *N*-glycosylation puzzle and reveal the importance of the conserved *N*-glycosylation of the mammalian SID-1 transmembrane family for RNA transport, RNA binding, proper functional localization, etc. These results may help to elucidate the regulatory pathways of the cellular function of the SID-1 transmembrane family.

RESULTS

The mammalian SID-1 transmembrane family is *N*-glycosylated

We searched for evolutionarily conserved (Asn-X-Ser/Thr, where X is any amino acid except for Pro) motifs in the amino-acid sequences of the mammalian SID-1 transmembrane family from different species using NetGlyc 1.0[32]. The prediction results show that the mammalian SID-1 transmembrane family contains 7-10 potential *N*-

glycosylation sites. Of these sites, 3-4 are located within the TMs, while the remaining sites are located in the ECD (based on human SIDT1 sequence, shown in Fig. 1A). However, whether these sites are *N*-glycosylated remains unknown. To verify the *N*-glycosylation status of human SIDT1, we first heterologously overexpressed SIDT1 in human embryonic kidney (HEK293T) cells and treated the cell lysates with Peptide-*N*-Glycosidase F (PNGase F) to study the enzymatic deglycosylation effect. As shown in the immunoblotting result, SIDT1 was found to have an approximate mass of 100 kDa. As expected, after treatment with PNGase F, the migration of SIDT1 was accelerated and the apparent molecular mass decreased to approximately 90 kDa (Fig. 1B). Similar results were obtained when we performed the same experiments with SIDT2, indicating that SIDT1 and SIDT2 are *N*-glycosylated (Fig. 1B), in agreement with previous studies[24,25].

Considering that *N*-glycosites of SIDT1 and SIDT2 are mainly located in the ECD, we also recombinantly obtained the truncated proteins ($SIDT1^{ECD}$ and $SIDT2^{ECD}$) from mammalian cells (HEK293F) and evaluated their *N*-glycosylation status. Immunoblot analysis reveals a broad band at approximately 50 kDa, and the width of the electrophoretic band is characteristic of glycosylated proteins and can be attributed to the heterogeneity of the carbohydrate moieties (Fig. 1C). However, after treatment with PNGase F, $SIDT1^{ECD}$ and $SIDT2^{ECD}$ appeared as a single 30 kDa band, and the apparent molecular mass decreased by ~20 kDa (Fig. 1C).

To determine the site-specific *N*-glycosylation of SIDT1, the SIDT1 protein recombinantly expressed in HEK293F cells with intact *N*-glycosylation was digested into peptides and the intact glycopeptides were analyzed with LC-MS/MS using EThcD mode. The workflow for site-specific *N*-glycosylation characterization of recombinant proteins is

shown in Supplementary Fig. 2A. We identified five extracellularly localized glycosylation sites (N57, N67, N83, N136, N282) out of the eight predicted *N*-glycosites of SIDT1, and the remaining three transmembrane-located sites were unoccupied. The occupancy of glycopeptides at each glycosylation site is shown in Fig. 1D. The *N*-glycosylation modification occurred mainly at N57, N67 and N83, with these three sites accounting for over 90% of the identified glycosylated peptides. We also performed the same analysis on recombinant human SIDT2, six *N*-glycosites (N27, N54, N60, N123, N141, N165) were identified and the occupancy of each glycosite is shown in Fig. 1e. Furthermore, using LC-MS/MS based intact glycopeptide mapping, we were able to identify over 100 types of *N*-linked glycans including paucimannose, high mannose, hybrid and complex-type glycans across the detected *N*-glycosites (Supplementary Fig. 2B, C), demonstrating the remarkable heterogeneity of *N*-glycosylation in human cells for both SIDT1 and SIDT2, in agreement with immunoblotting results.

Taken together, these results suggest that SIDT1 and SIDT2 are highly *N*-glycosylated. The total *N*-glycan moiety was ~20 kDa and the *N*-glycosites are located exclusively in the ECD.

Defective *N*-glycosylation can attenuate SIDT1-mediated RNA uptake

Previous studies have shown that the mammalian SID-1 transmembrane family appears to play several cell physiological roles by mediating cellular uptake and intracellular trafficking of oligonucleotides[12-15,18,19]. We postulated that *N*-glycosylation might be critical for SIDT1-mediated RNA transport. To test this hypothesis, we performed an RNA uptake assay using SIDT1, which has been identified to promote extracellular

siRNA and miRNA uptake.

To investigate the potential impact of *N*-glycosylation on SIDT1-mediated RNA transport, we generated a non-*N*-glycosylatable SIDT1 variant by genetic substitution of the native asparagines with glutamines, namely SIDT1$^{\Delta N\text{-glycan}}$. We overexpressed the wild-type SIDT1 and non-*N*-glycosylated SIDT1 (SIDT1$^{\Delta N\text{-glycan}}$) in HEK293T cells and incubated with biotinylated single-stranded RNA (ssRNA) or dsRNA, followed by streptavidin alkaline phosphatase (AP) staining[33]. We observed increased biotinylated RNA in cells expressing SIDT1 than in the control group (HEK293T cells transfected with empty vector pcDNA3.1(+)) (Fig. 2A). In contrast, HEK293T cells transfected with the SIDT1$^{\Delta N\text{-glycan}}$ variant showed a marked reduction in transported biotinylated RNA (Fig. 2A). The result show that the *N*-glycosylation support effective SIDT1-mediated RNA uptake.

To further confirm the role of *N*-glycosylation in SIDT1-mediated RNA uptake, pancreatic ductal adenocarcinoma (PANC1) cell line was used in this study, and the RNA uptake assay was performed as previously described[14]. The PANC1 cells were transfected with empty vector pcDNA3.1(+), wild-type SIDT1 or SIDT1$^{\Delta N\text{-glycan}}$, respectively. After incubation with synthesized Cy3-labeled RNA, RNA uptake was detected by fluorescence. Interestingly, as shown in Fig. 2B, incubation of cells with RNA in medium at pH 7.5 for 6 hours dramatically increased RNA uptake in wild-type SIDT1-transfected cells, in agreement with previous studies[14]. In contrast, overexpression of SIDT1$^{\Delta N\text{-glycan}}$ in PANC1 cells, which has similar expression levels to the wild-type SIDT1, showed a reduction in RNA uptake (Fig. 2B). Our results show that PANC1 cells expressing wild-type SIDT1 exhibited enhanced RNA uptake compared to SIDT1$^{\Delta N\text{-glycan}}$, which is

consistent with what was observed in the AP staining assay.

Furthermore, we functionally assess the effect of the transported siRNA. PANC1 cells transfected with empty vector pcDNA3.1(+), SIDT1 or SIDT1$^{\Delta N\text{-glycan}}$ were incubated with synthetic epidermal growth factor receptor (EGFR)-specific siRNA, and siRNA-induced gene silencing of EGFR was detected by Western blot. siRNA-induced gene silencing of EGFR was remarkably facilitated by wild-type SIDT1 overexpression (Supplementary Fig. 3). In contrast, siRNA-mediated gene silencing of EGFR was attenuated when cells were transfected with the SIDT1$^{\Delta N\text{-glycan}}$ variant (Supplementary Fig. 3). The results demonstrate that siRNA can induce gene silencing following the enhanced SIDT1-mediated uptake. Taken together, these results suggest that *N*-glycosylation of SIDT1 plays a critical role in promoting SIDT1-mediated RNA uptake and resulting in increased siRNA-mediated gene silencing efficacy.

_N_-glycosylation contributes to RNA binding and protein stability of SIDT1

It is well established that protein *N*-glycan moieties play a crucial role in mediating a wide range of intrinsic and extrinsic interactions[26]. There are several examples of the requirement for *N*-glycosylation in the formation of protein-protein interactions. For example, *N*-glycosylation of the vasopressin V1a receptor is required for optimal receptor-ligand binding, and *N*-glycosylation of the P2Y12 receptor is required for proper downstream Gi-mediated signaling[34,35]. Previous reports have shown that ECD of the SID-1 transmembrane family can directly bind to RNA, which is a critical activity for its involvement in RNA transport[23]. Our results suggest that SIDT1 is *N*-glycosylated at conserved N-X-S/T motifs located in the ECD and that defective *N*-glycosylation can

attenuate SIDT1-mediated RNA transport, leading us to speculate that RNA-binding is likely to be *N*-glycosylation dependent. To investigate this hypothesis, we performed both RNA pull-down and electrophoretic mobility shift assay (EMSA) to compare the binding of SIDT1 or SIDT1$^{\Delta N\text{-glycan}}$ to RNA.

First, we performed an RNA pull-down assay to identify the interaction of wild-type SIDT1 or SIDT1$^{\Delta N\text{-glycan}}$ with RNA. We performed immunoprecipitation (IP) with biotin-labeled single-stranded RNA (ssRNA) or dsRNA, and RNA-protein complexes were immunoprecipitated with antibodies against biotin. The amount of co-precipitated proteins was then measured by Western blot in HEK293T cells transfected with SIDT1 or SIDT1$^{\Delta N\text{-glycan}}$. Compared to wild-type SIDT1 transfected cells, we found that the RNA-bound complexes in SIDT1$^{\Delta N\text{-glycan}}$ transfected cells had significantly lower amounts of proteins (Fig. 3A). Importantly, these differences were not due to variations in protein levels, as demonstrated by consistent protein expression (Fig. 3A). Overexpression of SIDT1$^{\Delta N\text{-glycan}}$ greatly reduced the enrichment of the protein, suggesting that the absence of the conserved *N*-glycans affects the binding of SIDT1 to RNA.

Considering that the ECD of SIDT1 can bind directly to RNA, we further performed EMSA to assess the difference in binding of SIDT1^{ECD} with or without proper *N*-glycans to RNA. We were unable to obtain glycan-free SIDT1 proteins due to the large amount of precipitation caused by the deglycosylation with PNGase F. *N*-glycan-deficient or -intact SIDT1^{ECD} proteins (SIDT1$^{ECD\,N\text{-glycan-deficient}}$ and SIDT1$^{ECD\,N\text{-glycan-intact}}$) were obtained from HEK293F cells in the presence or absence of kifunensine, a potent inhibitor of α-mannosidase I, which inhibits *N*-glycan synthesis at the $Man_8GlcNAc_2$ (Man8) or $Man_9GlcNAc_2$ (Man9) stage[36]. We incubated 5'-fluorescein (FAM) labeled ssRNA with

increasing concentrations of SIDT1^{ECD} proteins and separated the bound and free forms of RNA on native polyacrylamide gels. After incubation of ssRNA with SIDT1$^{ECD\textit{N}\text{-glycan-intact}}$, we observed an unshifted band corresponding to unbound RNA and a compact shifted band presumably corresponding to the saturated RNA-protein complexes. These results showed a progressive decrease in ssRNA mobility with increasing protein concentration, indicating that SIDT1^{ECD} interacts directly with ssRNA (Fig. 3B). Importantly, no shift bands were observed when kifuensine was applied during SIDT1^{ECD} expression, suggesting that SIDT1^{ECD} with deficient *N*-glycosylation is unable to bind ssRNA under the above conditions, which is similar to the RNA pull-down results (Fig. 3B). Collectively, these results suggest that the *N*-glycosylation is critical for SIDT1 binding to RNA and for RNA transport.

Previous studies have shown that SIDT1 mediates RNA transport in lysosomes and pit cells of the gastric epithelium, where the ECD domain is exposed to the lumen of the lysosome and the acidic gastric environment[13,18]. Since *N*-glycosites are located in the ECD and glycans are generally known to protect against proteolysis[35,37], we postulate that *N*-glycosylation may function to maintain the protein stability of SIDT1 at low pH and protect it from degradation. To test this hypothesis, we examined the protein stability of SIDT1$^{ECD\textit{N}\text{-glycan-intact}}$ and SIDT1$^{ECD\textit{N}\text{-glycan-deficient}}$ at different pH values (pH 7.5, 5.5, and 3.5). We measured thermostability as a consequence of protein stability using differential scanning fluorometry (DSF). Temperature-dependent changes in intrinsic protein fluorescence revealed that the two SIDT1^{ECD} proteins with different *N*-glycosylation states were folded. The *N*-glycosylation deficiency of SIDT1^{ECD} caused a decrease in transition midpoint (Tm) of 4.7 °C at pH 7.5, 1.7 °C at pH 5.5, and 5.4 °C at pH 3.5 compared to

SIDT1$^{ECD\textit{N}\text{-glycan-intact}}$ with a Tm of 55.1 °C, 60.5 °C, and 61.1 °C at pH 7.5, 5.5, and 3.5, respectively (Fig. 3C). This indicates that the *N*-glycosylation of SIDT1 is essential for protein stabilization.

We then performed a comprehensive time-chase experiment to monitor the degradation of SIDT1^{ECD}. We incubated SIDT1$^{ECD\textit{N}\text{-glycan-intact}}$ or SIDT1$^{ECD\textit{N}\text{-glycan-deficient}}$ proteins at pH 7.5, 5.5, and 3.5 and then analyzed them on a 12% SDS-PAGE gel to visualize the relative mobility. Notably, incubation of SIDT1$^{ECD\textit{N}\text{-glycan-intact}}$ with low pH buffer for the experimental period of 0/1/2/4 hours did not result in degradation (Fig. 3D). Interestingly, incubation of SIDT1$^{ECD\textit{N}\text{-glycan-deficient}}$ at pH 3.5 for the same periods dramatically increased degradation compared to neutral conditions (Fig. 3D). The results suggest that the *N*-glycosylation protects SIDT1 from degradation in an acidic environment. Taken together, these results indicate that the *N*-glycosylation of SIDT1 enhances its stability and protects it from degradation in an acidic environment, which may be one of the reasons for the reduced RNA binding of *N*-glycan-deficient SIDT1.

Absence of *N*-glycan causes production of misfolded SIDT1, which is modulated by the endoplasmic reticulum quality control system (ERQC)

To further characterize the determinant responsible for the RNA uptake and binding defects observed upon removal of the *N*-glycan, we used *N*-glycosites mutant of SIDT1^{ECD}, designated as SIDT1$^{ECD\Delta\textit{N}\text{-glycan}}$. The small-scale expression studies were performed at the shake flask level to elucidate the effect of *N*-glycosylation on SIDT1^{ECD} protein secretion. We found that wild-type SIDT1^{ECD} folds and assembles correctly in HEK293T cells and is robustly secreted into the media. In contrast, SIDT1$^{ECD\Delta\textit{N}\text{-glycan}}$ caused a

significant and substantial secretion defect (Fig. 4A). We next sought to determine whether the secretion defect was due to a specific *N*-glycosite. Single amino acid mutants of each potential *N*-glycosite of SIDT1 (N57Q, N67Q, N83Q, N136Q, N282Q) were generated on SIDT1^{ECD}. Notably, the N83Q and N282Q SIDT1^{ECD} variants did not significantly affect secretion (Fig. 4B). The N57Q, N67Q and N136Q SIDT1^{ECD} variants were secreted abnormally and remained in the cytoplasm. The combined mutants also confirmed the above conclusions (Supplementary Fig. 4). This suggests that *N*-glycosylation is critical for successful folding and secretion of SIDT1^{ECD} and that the influence of each *N*-glycosite is different.

The secretion defect observed in the non-*N*-glycosylated SIDT1^{ECD} was remarkable. We speculated that this observation might be due to high production of non-*N*-glycosylated, misfolded SIDT1. The effect of *N*-glycosylation on secretion of SIDT1^{ECD} made us curious whether *N*-glycosylation would have the same effect on full-length SIDT1. To identify regulators whose expression was induced by *N*-glycan-deficient SIDT1, we further performed gene expression analysis on wild-type SIDT1 and SIDT1$^{\Delta N\text{-glycan}}$ overexpression HEK293F cells. Samples were subjected to RNA sequencing (RNA-seq) to reveal genes differences in SIDT1 overexpressing cells versus SIDT1$^{\Delta N\text{-glycan}}$ overexpressing cells.

We identified 90 down-regulated genes and 141 up-regulated genes in the comparative analysis of the samples (Supplementary Fig. 5A). RNA-seq results showed that expression of SIDT1$^{\Delta N\text{-glycan}}$ induced a substantial increase in the mRNA levels of ER stress-responsive transcripts, including those encoding hypoxia up-regulated protein 1 (HYOU1), binding immunoglobulin protein (BiP, HSPA5), etc. (Supplementary Fig. 5A). Our Reverse Transcription-Polymerase Chain Reaction (RT-PCR) experiments also

confirmed the above results (Supplementary Fig. 5C, D). In addition, Gene ontology (GO) analysis of the up-regulated genes showed that almost all the enriched pathways were associated with the ERQC, with 16 pathways, including unfolded protein response, endoplasmic reticulum stress, protein refolding, misfolded protein binding, molecular chaperone binding, etc. (Supplementary Fig. 5B).

The activated ERQC system can ultimately restore ER homeostasis by reducing the levels of target proteins and their mRNAs through multiple pathways. Therefore, we investigated the mRNA and protein levels of SIDT1 variants. The results showed that the mRNA level of SIDT1$^{\Delta N\text{-glycan}}$ was significantly lower than that of wild-type SIDT1 at 24 hours after transfection with the same amount of plasmid (Fig. 4C and Supplementary Fig. 6). In the time-course experiments of wild-type SIDT1 and SIDT1$^{\Delta N\text{-glycan}}$, the highest protein levels were reached at 48 hours after transfection. However, after 48 hours, the protein levels of wild-type SIDT1 remained essentially constant, whereas those of SIDT1$^{\Delta N\text{-glycan}}$ decreased significantly (Fig. 4D). Collectively, these results indicate that the non-*N*-glycosylated SIDT1 is severely misfolded. These severely misfolded non-*N*-glycosylated SIDT1 may cause ER stress, leading to the induction of the unfolded protein response (UPR) and regulated by the ERQC system.

Lack of *N*-glycosylation affects SIDT1 intracellular trafficking and surface expression

Cell surface expression of SIDT1 is critical for extracellular RNA uptake. In addition, our data have shown that the non-*N*-glycosylated SIDT1 undergoes severe misfolding, indicating that *N*-glycosylation is essential to ensure correct protein folding and

localization of SIDT1. Therefore, we hypothesized that the transport of SIDT1 to the cell surface would be critically impaired in the absence of *N*-glycosylation. To test this, we examined the wild-type SIDT1 and SIDT1$^{\Delta N\text{-glycan}}$ for cell surface expression by confocal microscopy in the absence and presence of saponin (a detergent that permeabilizes cell membranes without destroying them). The myc-tagged SIDT1 variants were transiently transfected into HEK293T cells to assess SIDT1 expression at the cell membrane using an antibody against myc as a marker for the membrane surface, since the antibody epitope is extracellular. We observed that in contrast to wild-type SIDT1, which has a good cell surface localization, SIDT1$^{\Delta N\text{-glycan}}$ was barely detected at the cell surface (Fig. 5A). Interestingly, in saponin-treated HEK293T cells, both wild-type SIDT1 and SIDT1$^{\Delta N\text{-glycan}}$ were largely localized to the cellular compartment (Fig. 5B).

Next, we visualized the status of intracellular retention of the protein by co-immunofluorescence analysis. We co-stained the Flag-tagged SIDT1 or SIDT1$^{\Delta N\text{-glycan}}$ variant with antibodies against the ER with the marker protein disulfide isomerase (PDI) or the Golgi marker GM130. We observed diffuse staining of SIDT1, either with or without the *N*-glycan, which was primarily localized to the ER (Fig. 5C), consistent with previous observations that 65% of SIDT1 is localized to the ER[38]. What's more, the wild-type SIDT1 stained diffusely in both the Golgi and the ER, consistent with a longer ER residence time and excessive post-translational modification, indicating that the protein has successfully completed the maturation pathway (Fig. 5C, D). In contrast, we did not detect SIDT1$^{\Delta N\text{-glycan}}$ co-localized with GM130, but instead it was predominantly located in the ER, suggesting that SIDT1$^{\Delta N\text{-glycan}}$ may be misfolded and retained in the ER (Fig. 5C, D). Taken together, these results indicate that *N*-glycosylation is critical for the correct

localization of SIDT1, and that removal of *N*-glycosylation impairs the trafficking of SIDT1 proteins to the plasma membrane and retains it predominantly in the ER, which agrees with the RNA-seq results (Supplementary Fig. 5). Consistent with this notion, the non-*N*-glycosylated SIDT1 variant were readily observed in immunofluorescence experiments, but were barely detectable at the plasma membrane and retained in the cytoplasm (Fig. 5A).

In conclusion, our data indicate that ECD-localized *N*-glycosylation is important for the intracellular trafficking and cell surface expression of SIDT1, thereby promoting further protein processing. Removal of the *N*-glycans resulted in the intracellular retention of SIDT1 and subsequently severe defects in RNA uptake activity.

Discussion

Protein *N*-glycosylation is by far the most ubiquitous post-translational modification and can significantly affect the properties and functions of target proteins by the addition of bulky, hydrophilic carbohydrate structures to specific asparagine residues[26]. *N*-glycosylation has previously been shown to regulate protein folding, solubility, stability and activity, protection from proteases, subcellular targeting, and other interactions[29,32]. Our sequence analysis revealed that *N*-glycosylation of SID1 transmembrane family members is conserved in most mammals (Fig. 1A and Supplementary Fig. 1), suggesting potentially functional contributions of *N*-glycosylation to the mammalian SID-1 transmembrane family. In this study, we analyzed the role of *N*-glycosylation in SIDT1-mediated RNA uptake function and explored the underlying molecular mechanisms. Thus, the evidence provides a direct link from *N*-glycosylation to SIDT1-mediated RNA uptake.

In agreement with previous studies, we verified that SIDT1 and SIDT2 are *N*-linked glycosylated by glycosidase digestion (PNGase F). We profiled the site-specific *N*-glycosylation of recombinant SIDT1 and SIDT2 proteins expressed from HEK293F cells. The occupancy at ECD-located *N*-glycosites of SIDT1 and SIDT2 (N57, N67, N83, N136, N282 for SIDT1; N27, N54, N60, N123, N141, N165 for SIDT2) was quantified. The results show that the putative transmembrane *N*-glycosites are not unoccupied. It is likely that the proximal putative *N*-glycosites could not be recognized by the oligosaccharyltransferase, since a minimum of 12 amino acid residues between the *N*-glycosylation consensus site and the transmembrane helix is required for efficient *N*-glycosylation[39].

Our results show that the occupancy of glycosylation at each *N*-glycosite is different, and the *N*-glycosylation of SIDT1 and SIDT2 in human cells displays remarkable heterogeneity, with paucimannose, high mannose, hybrid and complex-type glycans present across the *N*-glycosites. Research has shown that protein *N*-glycosylation patterns can change in disease. In non-alcoholic fatty liver disease (NAFLD) and non-alcoholic steatohepatitis (NASH), the glycosylation status of SLC transporters is alered[40]. The expression of non-glycosylated organic anion transporting polypeptides, OATP1B1/3 (SLCO1B1/3), OATP2B1 (SLCO2B1) and non-glycosylated Na^+-taurocholate co-transporting polypeptide (NTCP; SLC10A1) were found to be increased in NASH using gene array data and subsequent Western blot analysis of human liver donors[41]. In several diseases, SIDT1 and SIDT2 are implicated. SIDT1 plays a key role in breast, pancreatic, and non-small cell lung cancer[8,9,11]. Loss of function studies has demonstrated an essential role for SIDT2 in the regulation of glucose metabolism, lipid metabolism, antiviral

immunity, skeletal muscle homeostasis, and tumor development[5-10]. It's also implicated in neurodegenerative disorders like Alzheimer's[42]. It would therefore be interesting to determine whether *N*-glycosylation is altered in SIDT1- and SIDT2-related diseases.

A large body of evidence highlights an important role for *N*-glycosylation in the cell surface expression of biomolecules[31,37,43,44]. Our results show that complete deglycosylation of SIDT1 by site-directed mutagenesis results in a significant decrease in cell surface expression of the SIDT1, together with increased retention in the intracellular compartment (Fig. 5). Colocalization studies showed that non-*N*-glycosylated SIDT1 was localized predominantly to the ER and not to the Golgi apparatus, suggesting that *N*-glycosylation is important for the biosynthetic processing from the ER. In the absence of *N*-glycans, processing in the Golgi apparatus is prevented, thereby blocking the Golgi secretory pathway. Similar results were observed for the secretory expression of $SIDT1^{ECD}$, showing that non-*N*-glycosylated variant has a significant and substantial secretion defect (Fig. 4A). These results correlated with the transcriptional up-regulation of molecules HYOU1, HSPA5, etc (Supplementary Fig. 5), indicating cells undergoing ER stress and activation of pathways within the unfolded protein response. Our results indicate that *N*-glycosylation is required for efficient protein expression of SIDT1. However, the exact role of *N*-glycosylation, particularly the impact of different *N*-glycosites on SIDT1, still requires further investigation to be elucidated.

Another potential role of *N*-glycosylation is to affect the interaction between SIDT1 and RNA. Here, we show that the complete removal of *N*-glycans by mutagenesis disrupts the interaction of SIDT1 with RNA. The binding of *N*-glycan-deficient $SIDT1^{ECD}$ to RNA was significantly weaker than that of *N*-glycan-intact $SIDT1^{ECD}$, suggesting that *N*-glycans

play a critical role in shaping the SIDT1-RNA interaction. A likely explanation for the reduced RNA binding is that the *N*-glycans are involved in the binding of SIDT1 to RNA. Further single-molecule studies are needed to determine the detailed biochemical and biophysical properties of SIDT1 involved in RNA binding. Another plausible explanation is the reduced protein stability of *N*-glycan-deficient SIDT1 (Fig. 4C, D). Previous studies clearly show that dietary miRNAs are absorbed occurs in the stomach and that gastrically-enriched SIDT1 is the key molecule[18]. In the gastrointestinal tract, SIDT1 has the highest expression levels in the stomach and large intestine (including the cecum, colon and rectum), and these are the tissues exposed to the highest proteolytic activities in the body with various proteases derived from pancreatic secretion. Extracellular domain of SIDT1 in the apical membrane are therefore particularly susceptible to rapid degradation with loss of functionality. Indeed, our results suggest that *N*-glycosylation of SIDT1 confers resistance to the mimicked acidic gastric environment (pH 3.5, Fig. 4C, D).

Our results indicated that *N*-glycosylation is required for efficient SIDT1-mediated RNA uptake (Fig. 2), which may be attributed to the fact that *N*-glycosylation is required for correct subcellular localization of SIDT1. Removal of the *N*-glycans induced misfolding of SIDT1. Furthermore, the absence of *N*-glycosylation of SIDT1 disrupts SIDT1-RNA interactions, which may also explain why *N*-glycans play a role in SIDT1-mediated RNA uptake. These observations support the idea that the reduction in SIDT1-mediated RNA uptake in cells expressing *N*-glycan-deficient SIDT1 is probably due to a lack of available cell surface SIDT1. In addition, the *N*-linked glycans present on SIDT1 were critical for RNA binding and might play a role in regulating SIDT1 protein stability. It

would be interesting to further study whether the reduced RNA uptake is due to the aberrant glycan structure of SIDT1 or to the specific *N*-glycosite.

Over the past few decades, RNA-based therapies have developed rapidly compared to conventional drugs such as small molecules and proteins, and have many advantages, such as easier and faster design and production, cost-effectiveness, an expanded range of therapeutic targets, and flexible combinations of drug cocktails for personalized treatment[45-47]. RNA-based therapeutics, such as siRNA, miRNA, and mRNA, can silence gene expression, regulate target genes, or induce the expression of specific genes[48,49]. Exogenous dietary miRNAs can be transported to the pit cells in the stomach by the intrinsic carrier protein SIDT1 and then secreted as functional entities in exosomes[18]. This natural mammalian uptake pathway of dietary miRNAs can be easily exploited for oral delivery of therapeutic miRNAs, which may be an important direction for the future development of RNA-based medicine. Our findings reveal the effect of *N*-glycosylation on SIDT1-mediated RNA uptake and shed light on the development of oral delivery-based small RNA therapeutics.

Materials and Methods

Plasmid construction

The full-length cDNAs for human SIDT1 and human SIDT2 were synthesized by Genscript Company (SIDT1, Uniport: Q9NXL6; SIDT2, Uniport: Q8NBJ9). For protein expression and purification, the sequence encoding residues 23-310 of human SIDT1 and residues 22-292 of human SIDT2 were cloned into a modified pcDNA3.1(+) vector with a melittin signal sequence (MKFLVNVALVFMVVYISYIYA) at the N-terminus and a 6 x

His tag at the C-terminus. Full-length SIDT1 and SIDT2 with a C-terminal Flag tag or a N-terminal myc tag were subcloned into pcDNA3.1(+) vector. The SIDT1 mutants were generated by PCR-based mutagenesis method and cloned into this vector in the same way. The identity of each clone was verified by Sanger sequencing.

Protein expression and purification

$SIDT1^{ECD}$ and $SIDT2^{ECD}$ expression were performed in HEK293F cells (Invitrogen). Cells were cultured in OPM-293 CD05 medium (OPM Biosciences co., Ltd.) at 37 °C supplemented with 5% CO_2 in a ZCZY-CS8 shaker (Shanghai Zhichu Instrument co., Ltd.) at 120 rpm. When the cell density reached 2.5×10^6 to 3.0×10^6 cells per mL, the cells were transiently transfected with the expression plasmids. Approximately 1.5 mg of plasmids were pre-mixed with 4.5 mg of polyethylenimines (PEIs) (Polysciences) in 50 mL of fresh medium for 30 min before application. For transfection, 50 mL of the mixture was added to 1 liter of cell culture, and the transfected cells were harvested 72 hours after incubation. Cells were collected by double centrifugation and 6x His-tagged target protein in the supernatant was purified using the medium by Ni-NTA (Qiagen) affinity chromatography. Protein was eluted with buffer B containing 50 mM HEPES pH 7.5, 250 mM NaCl, and 250 mM imidazole. The eluate was then concentrated and purified by size exclusion chromatography on a Superdex 200 increase 10/300 column (GE Healthcare), pre-equilibrated with buffer C containing 20 mM HEPES pH 7.5, 100 mM NaCl and 0.1 mM tris (2-carboxyethyl) phosphine hydrochloride (TCEP). Peak fractions of the targets were confirmed by SDS-PAGE followed by Coomassie blue staining, and data analysis were performed using GraphPad Prism 9.0 software (GraphPad Software, San Diego, CA, USA).

Full-length SIDT1 expression was performed in HEK293F cells in the same manner. For protein expression and purification, 2 liters of cells were harvested 60 hours post-transfection, then the cells were lysed in lysis buffer containing 50 mM HEPES pH 7.5, 300 mM NaCl, 1 mM ethylenedinitrilotetraacetic acid (EDTA), and supplemented with protease inhibitor cocktail (MCE, Cat# HY-K0010) and 1 mM phenylmethylsulfonyl fluoride (PMSF). Cells were disrupted by continuous high-pressure cell disruption at 800 bars. Cells debris was removed by low-speed centrifugation for 30 minutes and the supernatant were further subjected to high-speed centrifugation at 150,000 g for 90 minutes using a Ti-45 rotor (Beckman), and the membrane component was collected. The membrane was resuspended and homogenized using a glass dounce homogenizer for 20 cycles on ice in solubilization buffer containing 50 mM HEPES pH 7.5, 300 mM NaCl, 1 mM EDTA, 2% (*w/v*) n-dodecyl-β-D-maltoside (DDM, Anatrace), 0.2% (*w/v*) cholesteryl hemisuccinate (CHS, Anatrace), protease inhibitor cocktail and solubilized at 4 °C with gentle agitation for 2 hours. The extraction was centrifuged at 39,000 g (Beckman) for 1 hour to remove the insoluble components, and supernatant was applied to incubate with anti-Flag affinity resin (Genscript) at 4 °C for 1.5 hours. The protein was eluted using buffer containing 50 mM HEPES pH 7.5, 300 mM NaCl, 0.01% (*w/v*) lauryl maltose neopentyl glycol (LMNG), 0.001% (*w/v*) CHS, and 500 μg/mL synthesized Flag peptide (Genscript). The eluent was further purified by SEC using a Superose 6 increase 10/300 column (GE Healthcare) pre-equilibrated with buffer containing 25 mM HEPES pH 7.5, 150 mM NaCl, 0.5 mM EDTA, 0.01% (*w/v*) LMNG, and 0.001% (*w/v*) CHS. Protein purity was examined by SDS-PAGE and visualized by Coomassie blue staining. Peak fractions were pooled and concentrated to 2 mg/mL, and then flash frozen in liquid nitrogen for

LC/MS analysis.

Plasmid of PNGase F was gifted from the laboratory of Fuquan Yang (Institute of Biophysics, Chinese Academy of Sciences) and a C-terminal Strep II tag was designed for purification. The plasmid was transformed into *E. coli* BL21 (DE3) cells. Cells were grown to an OD_{600} of 0.8 at 37 °C and then induced with 0.2 mM isopropyl-1-thio-D-galactopyranoside (IPTG). The cells were harvested by centrifugation after shaking at 16 °C for 20 hours and resuspended in buffer containing 50 mM Tris-HCl pH 8.0, 500 mM NaCl, and 1 mM PMSF, followed by disruption with a high-pressure homogenizer cell disrupter (JNBIO), and the lysate was centrifuged for 30 minutes at 18,000 g. The supernatant was loaded onto Strep-Tactin affinity beads (GE Healthcare) and eluted in buffer containing 50 mM Tris-HCl pH 8.0, 300 mM NaCl, and 2.5 mM desthiobiotin. The protein was subsequently loaded onto a Superdex 200 increase 10/300 column pre-equilibrated with buffer containing 20 mM Tris-HCl pH 8.0, 150 mM NaCl, and 0.5 mM TCEP. Purified proteins were assessed by SDS-PAGE and stored at -80 °C.

Transfection and Western blot

Transfections of cell monolayers were performed using the Lipofectamine 3000 (Invitrogen) in 6-well plates according to the manufacturer's instructions. Transfected cells were incubated at 37°C for 24 hours unless otherwise stated. To obtain cell lysates, cells were trypsinized, washed with phosphate-buffered saline (PBS), and lysed in lysis buffer with 50 mM Tris-HCl pH 7.5, 150 mM NaCl, 1 mM EDTA, 1.5 mM $MgCl_2$, 1% NP-40, 1.5 mM PMSF, and protease inhibitor cocktail (MCE, Cat# HY-K0010). Lysates were cleared by centrifugation at 14000 g and 4 °C for 10 minutes. The total protein in the supernatant was quantified using the bicinchoninic acid assay (BCA) kit (Beijing TianGen

Biotechnology Co., Ltd.). For each sample, equivalent amounts of total protein were evaluated during the analysis. Cell lysates or media were denatured by boiling in 4 x SDS-PAGE sample loading buffer (200 mM Tris-HCl pH 6.8, 40% (*v/v*) glycerol, 8% (*w/v*) SDS, 0.008% (*w/v*) bromophenol blue, and 20% (*v/v*) β-mercaptoethanol), separated on 10% or 12.5% SDS-PAGE gels, and transferred to PVDF membranes. Blots were imaged after incubation with appropriate primary and secondary antibodies using the Tanon-5100 Fluorescent Imaging System (Tanon Science & Technology), followed by quantification as required using ImageJ as appropriate.

De-*N*-glycosylation analysis

Whole cell lysates (WCLs) and culture medium were obtained from HEK293T cells transfected with SIDT1 or SIDT2. The combinations were subjected to the de-*N*-glycosylation analysis to confirm the extent of glycosylation using PNGase F, which cleaves the innermost *N*-acetyl-glucosamine (GlcNAc) and asparagine residues (Asn, N). The samples were treated with PNGase F at an enzyme-to-protein ratio of 1:50 (*w/w*) at 37 °C for 3 hours. The reaction mixture was studied on 10% SDS-PAGE to check the degree of glycosylation of the recombinant proteins.

In-solution digestion of samples

The purified samples were digested into peptides as previously described[50]. Briefly, samples were reduced with DTT at a final concentration of 10 mM at 30 °C for 1 hour. The resulting free thiols were alkylated with IAM at a final concentration of 40 mM for 45 minutes at room temperature (RT) in the dark. The same amount of DTT was then added to remove excess IAM at 30 °C for 30 minutes. Proteins were then digested with Lys-C

(Wako Pure Chemical Industries, Osaka, Japan) at an enzyme-to-protein ratio of 1: 100 (*w/w*) at 37 °C for 3 hours. After dilution with 50 mM Tris-HCl pH 8.0, samples were digested with sequencing grade modified trypsin (Promega, Madison, WI, USA) at an enzyme-to-protein ratio of 1:50 (*w/w*) at 37 °C overnight. Enzymatic digestion was stopped with formic acid (FA) and the supernatant was collected after centrifugation at 20,000 × g for 20 minutes. Peptides were desalted on HLB cartridges (Waters, Milford, MA, USA) and dried in a benchtop centrifugal vacuum concentrator (Labconco, MO, USA).

LC-MS/MS analysis

Peptide samples were dissolved in 0.1% FA and analyzed on the Orbitrap Eclipse Tribrid Mass spectrometer (Thermo Fisher Scientific) coupled to an Easy-nLC 1200 HPLC system (Thermo Fisher Scientific). Samples were separated on a fused silica trap column (100 μm ID x 2 cm) in-house packed with reversed-phase silica (Reprosil-Pur C18 AQ, 5 μm, Dr. Maisch GmbH, Baden-Wuerttemberg, Germany) coupled to an analytical column (75 μm ID x 20 cm) packed with reversed-phase silica (Reprosil-Pur C18 AQ, 3 μm, Dr. Maisch GmbH). The peptides were analyzed with 103 min gradient (buffer A: 0.1% FA in H_2O, buffer B: 80% ACN, 0.1% FA in H_2O) at a flow rate of 300 nL/minutes (4-11% B, 4 min; 11-22% B, 32 minutes; 22-32% B, 31 minutes; 32-42% B, 23 minutes; 42-95% B, 3 minutes; 95% B, 10 minutes). MS data were acquired in data-dependent acquisition mode. The cycle time was set as 3 seconds (s). The spray voltage of the nano-electrospray ion source was 2.0 kV, with no sheath gas flow, the heated capillary temperature was 320 °C. An MS1 scan was acquired from 350 to 2000 m/z (60,000 resolution, $4e^5$ AGC, normalized AGC=100%, maximum injection time=50 ms) followed by EThcD MS/MS acquisition of

the precursors in an order of intensity and detection in the Orbitrap (30, 000 resolution, 4e5 AGC, normalized AGC=800%, maximum injection time=200 ms).

All raw data files were searched against the UniProt human reviewed protein database with target protein sequences and common contaminants, using the PTMcentric search engine Byonic (version 3.11.3, Protein Metrics)[51] incorporated in Proteome Discoverer (PD 2.2). Trypsin was selected as the enzyme and two maximum missed cleavages were allowed. Searches were performed with a precursor mass tolerance of 10 ppm and a fragment mass tolerance of 0.02 Da. Static modifications consisted of carbamidomethylation of cysteine residues (+57.02146 Da). Dynamic modifications consisted of the oxidation of methionine residues (+15.99492 Da), deamidation of asparagine and glutamine (+0.98402 Da), and *N*-glycosylation on asparagine. Oxidation and deamidation were set as "rare" modifications, and *N*-glycosylation was set as a "common" modification through Byonic node. Two rare modifications and one common modification were allowed. 182 human *N*-glycans embedded in Byonic, which contains 309 glycan entities, was used. Results were filtered to a 1% protein FDR as set in the Byonic parameters, and data were further processed to 1% FDR at the PSM level using the 2D-FDR score (a simple variation of the standard target-decoy strategy that estimates and controls PSM and protein FDRs simultaneously)[52]. Only those *N*-glycopeptides with Byonic score >100 and |logProb| > 1 were reported. Each glycopeptide identified should have the consensus motif N-X-S/T, X≠P. The filtering criteria have been reported to result in confident glycosite assignment at glycopeptide spectral match level[53].

Cell-based RNA uptake Assays

Cell-based RNA uptake assays were performed in cultured cells using a previously

described method[14,18]. Briefly, SIDT1 and SIDT1$^{\Delta N\text{-glycan}}$ plasmids were transfected into HEK293T or PANC1 cells in 6-well plates using Lipofectamine 3000 (Invitrogen). After 24 hours, HEK293T cells were washed twice with 1 mL PBS. RNA uptake was performed at RT for 10 minutes by incubating cells with 15 mM biotinylated ssRNA and dsRNA (encoding same sequences 5' -TCGCTTGGTGCAGATCGGGAC- 3') in 1 mL fetal bovine serum (FBS)-free DMEM, and the pH of the culture medium was adjusted with hydrochloric acid to 5.5. RNA uptake assays of SIDT1 and SIDT1$^{\Delta N\text{-glycan}}$ transfected PANC1 cells were performed at 37 °C for 6 hours or RT for 10 minutes by incubating cells with 40 pmol/mL Cy3-labeled dsRNA (5' -TCGCTTGGTGCAGATCGGGAC- 3') or unlabeled EGFR-specific siRNA in 1 mL FBS-free DMEM, and the pH of the culture medium was adjusted with hydrochloric acid to 3.5. The reaction was stopped by three washes with PBS and incubated with FBS-free medium containing 0.2 mg/mL RNase A (Thermo Fisher Scientific, Cat# 12091021) for 1 hours to digest the extracellularly attached RNAs. Cells were washed three times, and total transported RNA and protein were detected.

Streptavidin AP staining

After the cell-based RNA uptake assay, streptavidin AP staining was performed. Cells were fixed with 4% paraformaldehyde and permeabilized with 0.5% saponin for 10 minutes and then blocked with 3% bovine serum albumin (BSA). Then incubated with AP-conjugated streptavidin at 4 °C overnight. The plates were colorized with NBT/BCIP Substrate Solution (ThermoFisher, Cat#34042) at RT for 10 minutes. And cells were imaged with the Leica DFC365 FX fluorescence microscopy and analyzed with Image J.

RNA isolation and RT-PCR

Total RNA was separately extracted from the HEK293T cells of each indicated group. According to the manufacturer's recommended procedure, an RNAeasy™ kit (Beyotime Biotechnology, Cat# R0026;) was used to extract total RNA. Real-time PCR was carried out after the total RNA was extracted and reverse transcribed to cDNA using an RT-PCR kit (Vazyme Biotech, Cat#P611-01) according to the manufacturer's instructions. PCR experiments were run in triplicate using 60 ng of cDNA per reaction and 0.2 μM forward and reverse primers with 2× ChamQ SYBR Color qPCR Master Mix (Vazyme Biotech, Cat#Q431-02) on a Bio-Rad CFX 96 system (Bio-Rad, USA). The PCR cycling conditions consisted of an initial 30 s of denaturation at 95°C, followed by 40 cycles of 10 s of denaturation at 95°C and 30 s of annealing/elongation. The expression levels of target genes were normalized to glyceraldehyde-3-phosphate dehydrogenase (GAPDH) as a reference gene, and target gene expression was calculated by the $2^{-\Delta\Delta CT}$ method[54]. The control group was used for normalization, and the results are expressed as the fold change.

RNA Pull-Down

Empty vector pcDNA3.1(+), wild-type SIDT1, or SIDT1$^{\Delta N\text{-glycan}}$ transfected HEK293T cells were washed with PBS and lysed in RIPA buffer (25 mM Tris-HCl pH 7.4, 150 mM NaCl, 1% NP40) at RT for 30 minutes. WCLs were incubated (rotated) at 4 °C for 2 hours with 0.4 nmol biotinylated ssRNA or dsRNA encoding same sequences (5' -TCGCTTGGTGCAGATCGGGAC- 3') and 10 μL streptavidin-agarose in binding buffer containing 20 mM HEPES pH 7.4, 100 mM KCl, 0.5 mM EDTA, 1.5 mM $MgCl_2$, 20% (*v/v*) glycerol, 1 mM DTT, and protease inhibitor cocktail (MCE, Cat#HY-K0010). The binding reaction was terminated by centrifugation at 5000 rpm for 30 s and washing the resins with 1 mL of washing buffer 5 times. After the complete removal of the washing

buffer, 4 × SDS-PAGE sample buffer was added to the resins and heated at 95 °C for 10 minutes.

EMSA

The interaction between SIDT1$^{ECD\textit{N}\text{-glycan-intact}}$ or SIDT1$^{ECD\textit{N}\text{-glycan-deficient}}$ and ssRNA were examined by EMSAs. The ssRNA (5'-UCGCUUGGUGCAGAUCGGGAC-3') labeled at the 5' end with FAM was synthesized by Genscript co., Ltd. For the EMSA, increasing amounts of the SIDT1^{ECD} proteins (1.25, 2, 2.5, 5, and 10 μM) were incubated with 2.5 μM FAM-labeled ssRNA in a reaction EMSA buffer containing 40 mM Tris-HCl pH 5.5, (adjusted by acetate), 100 mM NaCl, 2.5 mM EDTA and 5 % (*v/v*) glycerol to a total volume of 20 μl at RT for 30 minutes. The obtained products were then resolved on 5 % native acrylamide gels (37.5:1 for acrylamide: bisacrylamide) in 1x Tris-acetate-EDTA (TAE) running buffer (pH 5.5) under an electric field of 10 V/cm for about 20 minutes on ice. The gel was visualized and analyzed by the Tanon-5100 Fluorescent Imaging System and Image J software.

DSF

The thermal stability was performed using Tycho NT.6 (NanoTemper Technologies). SIDT1$^{ECD\textit{N}\text{-glycan-intact}}$ and SIDT1$^{ECD\textit{N}\text{-glycan-deficient}}$ were diluted to a final concentration of 0.25 mg/mL at various pH (pH 7.5, 5.5, and 3.5), and analyzed in triplicates in capillary tubes. Protein unfolding was monitored using the intrinsic fluorescence at 350 and 330 nm with temperature gradient from 35 to 95 °C at a rate of 30 K/minutes. Data analysis, data smoothing, and the calculation of derivatives involved using the internal evaluation features of the Tycho instrument.

Time-course Experiments

To assess the effect of *N*-glycosylation on the protein stability of SIDT1, SIDT1$^{ECD\mathit{N}\text{-glycan-intact}}$ and SIDT1$^{ECD\mathit{N}\text{-glycan-deficient}}$ were exposed to the various pH buffer (pH 7.5, 5.5, and 3.5). The reaction was stopped after 0/1/2/4 hours incubation at RT by adding 4 x SDS-PAGE sample buffer. Proteins were heated at 95 °C for 10 minutes and separated by SDS-PAGE.

Enzyme-Linked Immunosorbent Assay (ELISA)

WCLs obtained from HEK293F cells transfected with empty vector pcDNA3.1(+), wild-type SIDT1, and SIDT1$^{\Delta\mathit{N}\text{-glycan}}$. The total protein in the supernatant was quantified using the BCA kit (Beijing TianGen Biotechnology Co., Ltd.). A clear flat bottom Maxisorp 96-well plate (Thermo Fisher Scientific, USA) was coated with anti-SIDT1 antibody (custom-generated, Yurogen Biosystems, Wuhan, China) at 50 μg/mL (50 μL/well) in ELISA coating buffer containing 15 mM Na_2CO_3/35 mM $NaHCO_3$ pH 9.6, 3 mM NaN_3 overnight at 4 °C. The plate was then blocked with 3% BSA for 1 hours at 37 °C, followed by incubation with WCLs for 2 hours at 37 °C. After three washes, the portion of the plate were overnight incubated with the anti-Flag antibody (Abclonal; 1:1000) in 3 % BSA at 4 °C, followed by the anti-mouse HRP secondary antibody (1:3000, Abclonal). Between antibodies, the plate was washed three times. Then the plate was developed using the TMB substrate and stop solution (Beyotime Biotechnology), and the plate was read at 450 nm. Graphs were plotted in GraphPad Prism 9.0 software.

RNA-Seq Library Construction, Sequencing, and Data Analyses

The HEK293F cells of pCDNA3.1(+), wild-type SIDT1 and SIDT1$^{\Delta\mathit{N}\text{-glycan}}$ transfected

cells were sent to Seqhealth Technology Co., Ltd. (Wuhan, China). Briefly, total RNA was extracted using a Trizol reagent (Invitrogen, USA) and was used for stranded RNA sequencing library preparation using a KCTM Stranded mRNA Library Prep Kit for Illumina® following the manufacturer's instruction. PCR products corresponding to 200-500 base pairs were enriched, quantified, and finally sequenced on a DNBSEQ-T7 sequencer (PE150, MGI). Reads were mapped to the Cyprinus carpio genome using STAR (version 2.5.3a) with default parameters[55]. The mapped reads were analyzed by feature Counts (Subread-1.5.1; Bioconductor)[56]. Differential expression genes were estimated by the edgeR package (version 3.12.1)[57]. The genes with low expression (CPM (counter-per-million) <1 in three or more samples) were excluded from downstream analysis. The resulting genes were considered as differentially expressed genes (DEGs) if FDR s 0.05 and |log2 (fold-change) | ≥1. For further analysis of the DEGs, we carried out a GO enrichment using KoBAS (version 2.1.1)[58] to identify the ER stress-related pathways that were significantly enriched following SIDT1$^{\Delta N\text{-glycan}}$ transfected.

Immunofluorescence microscopy

Monolayers of HEK293T cells grown on coverslips were transfected as described above. After 24 hours of transfection, culture media was removed and the coverslips were washed with PBS. The cells were then fixed with 4% paraformaldehyde at RT for 10 minutes and then incubated with 0.5% saponin for 10 minutes to permeabilize the cells. Coverslips were then incubated in a blocking solution of 3% BSA at RT for 1 hours. Cells were labeled overnight with the anti-Flag, or anti-myc antibody (Abclonal; 1:500) in 3 % BSA at 4 °C, followed by either the anti-PDI (Beyotime Biotechnology; 1:200) or anti-GM130 antibody (Beyotime Biotechnology; 1:200). Between antibodies, the coverslips were washed three

times with PBS. The secondary antibody (Alexa Fluor 647-conjugated anti-mouse and Alexa Fluor 488-conjugated anti-rabbit, Abclonal; 1:500) were used to incubate cells at RT in darkness for 1 hours. Both secondary antibodies, Alexa Fluor 647-conjugated anti-mouse and Alexa Fluor 488-conjugated anti-rabbit (Abclonal; 1:500) were applied simultaneously in the 3% BSA solution for 1 hours at RT. The coverslips were then washed three times with PBS and labeled with 2-(4-Amidinophenyl)-6-indolecarbamidine dihydrochloride (DAPI) (Beyotime Biotechnology) for 10 minutes at RT. Images were obtained with a Zeiss LSM 980 scanning confocal microscope. The images were processed with ZEN software (Carl Zeiss).

Quantification and statistical analysis

Measurements were performed in ImageJ (National Institutes of Health). Quantification and data analysis were performed with GraphPad Prism. The statistical details of experiments can be found in figure legends. All experiments were repeated independently for more than three times. All statistic values were displayed as means ± SD, the statistical significance in this study is determined by One-way analysis of variance (ANOVA) followed by Tukey's correction or the unpaired, two-tailed Student's *t*-test, $p > 0.05$ is set to not significant, *$p < 0.05$, **$p < 0.01$, ***$p < 0.001$, ****$p < 0.0001$.

Data availability

The mass spectrometric data have been deposited to the ProteomeXchange Consortium (http://proteomecentral.proteomexchange.org) via the iProX partner repository[59,60] with the dataset identifier PXD043824. The link access to the raw data is https://proteomecentral.proteomexchange.org/cgi/GetDataset?ID=PXD043824. The data

that support this study are available within the article and its Supplementary Information files. Source data are provided with this paper.

Acknowledgements

We thank Qipeng Zhang for valuable assistance and discussion of RNA uptake assay, and Shoubing Zhan for helpful assistance of RT-PCR. We also thank Tongyang Zhu and the National Key Laboratory of Pharmaceutical Biotechnology at Nanjing University in the technical assistance. We are grateful to Jifeng Wang from the Laboratory of Proteomics, Institute of Biophysics, Chinese Academy of Sciences for his help with mass spectrometric data acquisition. This work was supported by funds from the National Key Research and Development Program of China (2018YFA0507103), National Natural Science Foundation of China (grant No. 32270139 to X.J.).

Author contributions

T.Y., H.X., L.Z. and X.J. designed the experiments. T.Y., H.X., X.C., L.Z. and J.W. performed the experiments. Y.T., H.X., L.Z., F.Y. and C.Z. analyzed the data. T.Y., H.X., L.Z., H.G. and X.J. wrote the manuscript.

Competing interests

The authors declare no competing interests.

Corresponding authors

Correspondence to Chenyu Zhang, Fuquan Yang, Xiaoyun Ji.

Additional information

The Supplementary Material for this article can be found online at:

REFERENCES

1. Winston, W.M., Molodowitch, C. & Hunter, C.P. Systemic RNAi in C-elegans requires the putative transmembrane protein SID-1. *Science* **295**, 2456-2459 (2002).
2. Hunter, C.P. et al. Systemic RNAi in Caenorhabditis elegans. *Cold Spring Harbor Symposia on Quantitative Biology* **71**, 95-100 (2006).
3. Shih, J.D., Fitzgerald, M.C., Sutherlin, M. & Hunter, C.P. The SID-1 double-stranded RNA transporter is not selective for dsRNA length. *Rna* **15**, 384-390 (2009).
4. Shih, J.D. & Hunter, C.P. SID-1 is a dsRNA-selective dsRNA-gated channel. *Rna* **17**, 1057-1065 (2011).
5. Gao, J., Gu, X., Mahuran, D.J., Wang, Z. & Zhang, H. Impaired glucose tolerance in a mouse model of sidt2 deficiency. *PLoS One* **8**, e66139 (2013).
6. Gao, J., Yu, C., Xiong, Q., Zhang, Y. & Wang, L. Lysosomal integral membrane protein Sidt2 plays a vital role in insulin secretion. *Int J Clin Exp Pathol* **8**, 15622-31 (2015).
7. Andaleon, A., Mogil, L.S. & Wheeler, H.E. Gene-based association study for lipid traits in diverse cohorts implicates BACE1 and SIDT2 regulation in triglyceride levels. *Peerj* **6**(2018).
8. Nguyen, T.A. et al. SIDT2 RNA Transporter Promotes Lung and Gastrointestinal Tumor Development. *Iscience* **20**, 14-+ (2019).
9. Wang, Y. et al. Integrated Bioinformatics Data Analysis Reveals Prognostic Significance Of SIDT1 In Triple-Negative Breast Cancer. *Onco Targets Ther* **12**, 8401-8410 (2019).
10. Xiong, Q.Y., Xiong, C.Q., Wang, L.Z. & Gao, J.L. Effect of sidt2 Gene on Cell Insulin Resistance and Its Molecular Mechanism. *Journal of Diabetes Research* **2020**(2020).
11. Tian, Y. et al. Correlation of SIDT1 with Poor Prognosis and Immune Infiltration in Patients with Non-Small Cell Lung Cancer. *Int J Gen Med* **15**, 803-816 (2022).
12. Nguyen, T.A. et al. SIDT2 Transports Extracellular dsRNA into the Cytoplasm for Innate Immune Recognition. *Immunity* **47**, 498-+ (2017).
13. Nguyen, T.A. et al. SIDT1 Localizes to Endolysosomes and Mediates Double-Stranded RNA Transport into the Cytoplasm. *Journal of Immunology* **202**, 3483-3492 (2019).
14. Duxbury, M.S., Ashley, S.W. & Whang, E.E. RNA interference: A mammalian SID-1 homologue enhances siRNA uptake and gene silencing efficacy in human

cells. *Biochemical and Biophysical Research Communications* **331**, 459-463 (2005).
15. Elhassan, M.O., Christie, J. & Duxbury, M.S. Homo sapiens Systemic RNA Interference-defective-1 Transmembrane Family Member 1 (SIDT1) Protein Mediates Contact-dependent Small RNA Transfer and MicroRNA-21-driven Chemoresistance. *Journal of Biological Chemistry* **287**, 5267-5277 (2012).
16. Rupaimoole, R. & Slack, F.J. MicroRNA therapeutics: towards a new era for the management of cancer and other diseases. *Nat Rev Drug Discov* **16**, 203-222 (2017).
17. Zhou, Z. et al. Decreased HD-MIR2911 absorption in human subjects with the SIDT1 polymorphism fails to inhibit SARS-CoV-2 replication. *Cell Discov* **6**, 63 (2020).
18. Chen, Q. et al. SIDT1-dependent absorption in the stomach mediates host uptake of dietary and orally administered microRNAs. *Cell Res* **31**, 247-258 (2021).
19. Takahashia, M. et al. SIDT2 mediates gymnosis, the uptake of naked single-stranded oligonucleotides into living cells. *Rna Biology* **14**, 1534-1543 (2017).
20. Morell, M. et al. SIDT1 plays a key role in type I IFN responses to nucleic acids in plasmacytoid dendritic cells and mediates the pathogenesis of an imiquimod-induced psoriasis model. *EBioMedicine* **76**, 103808 (2022).
21. Aizawa, S. et al. Lysosomal putative RNA transporter SIDT2 mediates direct uptake of RNA by lysosomes. *Autophagy* **12**, 565-578 (2016).
22. Aizawa, S. et al. Lysosomal membrane protein SIDT2 mediates the direct uptake of DNA by lysosomes. *Autophagy* **13**, 218-222 (2017).
23. Li, W., Koutmou, K.S., Leahy, D.J. & Li, M. Systemic RNA Interference Deficiency-1 (SID-1) Extracellular Domain Selectively Binds Long Double-stranded RNA and Is Required for RNA Transport by SID-1. *J Biol Chem* **290**, 18904-13 (2015).
24. Gao, J.L., Gu, X.F. & Zhang, H.W. SID1 transmembrane family, member 2 (Sidt2) A novel lysosomal membrane protein. *Biochemical and Biophysical Research Communications* **402**, 588-594 (2010).
25. Pratt, A.J., Rambo, R.P., Lau, P.W. & MacRae, I.J. Preparation and characterization of the extracellular domain of human Sid-1. *PLoS One* **7**, e33607 (2012).
26. Schjoldager, K.T., Narimatsu, Y., Joshi, H.J. & Clausen, H. Global view of human protein glycosylation pathways and functions. *Nat Rev Mol Cell Biol* **21**, 729-749 (2020).
27. Roth, J. et al. Protein N-glycosylation, protein folding, and protein quality control. *Mol Cells* **30**, 497-506 (2010).
28. OConnor, S.E. & Imperiali, B. Modulation of protein structure and function by asparagine-linked glycosylation. *Chemistry & Biology* **3**, 803-812 (1996).
29. Mitra. N-linked oligosaccharides as outfitters for glycoprotein folding, form and function (vol 31, pg 156, 2006). *Trends in Biochemical Sciences* **31**, 251-251 (2006).
30. Esmail, S. & Manolson, M.F. Advances in understanding N-glycosylation structure, function, and regulation in health and disease. *Eur J Cell Biol* **100**, 151186 (2021).

31. Rowland, R. & Brandariz-Nunez, A. Analysis of the Role of N-Linked Glycosylation in Cell Surface Expression, Function, and Binding Properties of SARS-CoV-2 Receptor ACE2. *Microbiol Spectr* **9**, e0119921 (2021).
32. Gupta, R. & Brunak, S. Prediction of glycosylation across the human proteome and the correlation to protein function. *Pac Symp Biocomput*, 310-22 (2002).
33. Long, H. et al. Interaction of RAGE with alpha-synuclein fibrils mediates inflammatory response of microglia. *Cell Rep* **40**, 111401 (2022).
34. Zhong, X.T., Kumar, R., Seehra, J. & Kriz, R. N-linked glycosylation of platelet P2Y12 ADP receptor is essential for signal transduction but not for ligand binding or cell surface expression. *Faseb Journal* **18**, C31-C31 (2004).
35. Stelzl, T., Geillinger-Kastle, K.E., Stolz, J. & Daniel, H. Glycans in the intestinal peptide transporter PEPT1 contribute to function and protect from proteolysis. *Am J Physiol Gastrointest Liver Physiol* **312**, G580-G591 (2017).
36. Zhou, Q. et al. Development of a simple and rapid method for producing non-fucosylated oligomannose containing antibodies with increased effector function. *Biotechnology and Bioengineering* **99**, 652-665 (2008).
37. Hayashi, H. & Yamashita, Y. Role of N-glycosylation in cell surface expression and protection against proteolysis of the intestinal anion exchanger SLC26A3. *Am J Physiol Cell Physiol* **302**, C781-95 (2012).
38. Takahashi, M., Seki, M., Nashimoto, M. & Kabuta, T. Perturbing the Normal Level of SIDT1 Suppresses the Naked ASO Effect. *J Nucleic Acids* **2021**, 2458470 (2021).
39. Nilsson, I. & Vonheijne, G. Determination of the Distance between the Oligosaccharyltransferase Active-Site and the Endoplasmic-Reticulum Membrane. *Journal of Biological Chemistry* **268**, 5798-5801 (1993).
40. Aguilar-Olivos, N.E. et al. The nuclear receptor FXR, but not LXR, up-regulates bile acid transporter expression in non-alcoholic fatty liver disease. *Annals of Hepatology* **14**, 487-493 (2015).
41. Clarke, J.D., Novak, P., Lake, A.D., Hardwick, R.N. & Cherrington, N.J. Impaired N-linked glycosylation of uptake and efflux transporters in human non-alcoholic fatty liver disease. *Liver International* **37**, 1074-1081 (2017).
42. Fujiwara, Y. et al. Pathology-associated change in levels and localization of SIDT2 in postmortem brains of Parkinson's disease and dementia with Lewy bodies patients. *Neurochemistry International* **152**(2022).
43. Fischer, K., Topallar, S., Kraatz, F., Groschup, M.H. & Diederich, S. The role of N-linked glycosylation in proteolytic processing and cell surface transport of the Cedar virus fusion protein. *Virol J* **19**, 136 (2022).
44. Sun, R., Kim, A.M.J., Murray, A.A. & Lim, S.O. N-Glycosylation Facilitates 4-1BB Membrane Localization by Avoiding Its Multimerization. *Cells* **11**(2022).
45. Shin, H. et al. Recent Advances in RNA Therapeutics and RNA Delivery Systems Based on Nanoparticles. *Advanced Therapeutics* **1**(2018).
46. Chakraborty, C., Sharma, A.R., Sharma, G. & Lee, S.S. Therapeutic advances of miRNAs: A preclinical and clinical update. *Journal of Advanced Research* **28**, 127-138 (2021).

47. Setten, R.L., Rossi, J.J. & Han, S.P. The current state and future directions of RNAi-based therapeutics (vol 18, pg 421, 2019). *Nature Reviews Drug Discovery* **19**, 290-290 (2020).
48. Carthew, R.W. & Sontheimer, E.J. Origins and Mechanisms of miRNAs and siRNAs. *Cell* **136**, 642-655 (2009).
49. Sahin, U., Kariko, K. & Tureci, O. mRNA-based therapeutics - developing a new class of drugs. *Nature Reviews Drug Discovery* **13**, 759-780 (2014).
50. Li, J.R. et al. Comprehensive Evaluation of Different TiO2-Based Phosphopeptide Enrichment and Fractionation Methods for Phosphoproteomics. *Cells* **11**(2022).
51. Bern, M., Kil, Y.J. & Becker, C. Byonic: advanced peptide and protein identification software. *Curr Protoc Bioinformatics* **Chapter 13**, 13 20 1-13 20 14 (2012).
52. Bern, M.W. & Kil, Y.J. Two-Dimensional Target Decoy Strategy for Shotgun Proteomics. *Journal of Proteome Research* **10**, 5296-5301 (2011).
53. Lee, L.Y. et al. Toward Automated N-Glycopeptide Identification in Glycoproteomics. *Journal of Proteome Research* **15**, 3904-3915 (2016).
54. Bustin, S.A. et al. The MIQE guidelines: minimum information for publication of quantitative real-time PCR experiments. *Clin Chem* **55**, 611-22 (2009).
55. Dobin, A. et al. STAR: ultrafast universal RNA-seq aligner. *Bioinformatics* **29**, 15-21 (2013).
56. Liao, Y., Smyth, G.K. & Shi, W. featureCounts: an efficient general purpose program for assigning sequence reads to genomic features. *Bioinformatics* **30**, 923-930 (2014).
57. Robinson, M.D., McCarthy, D.J. & Smyth, G.K. edgeR: a Bioconductor package for differential expression analysis of digital gene expression data. *Bioinformatics* **26**, 139-140 (2010).
58. Wu, J.M., Mao, X.Z., Cai, T., Luo, J.C. & Wei, L.P. KOBAS server: a web-based platform for automated annotation and pathway identification. *Nucleic Acids Research* **34**, W720-W724 (2006).
59. Ma, J. et al. iProX: an integrated proteome resource. *Nucleic Acids Res* **47**, D1211-D1217 (2019).
60. Chen, T. et al. iProX in 2021: connecting proteomics data sharing with big data. *Nucleic Acids Res* **50**, D1522-D1527 (2022).

Figure Legends:

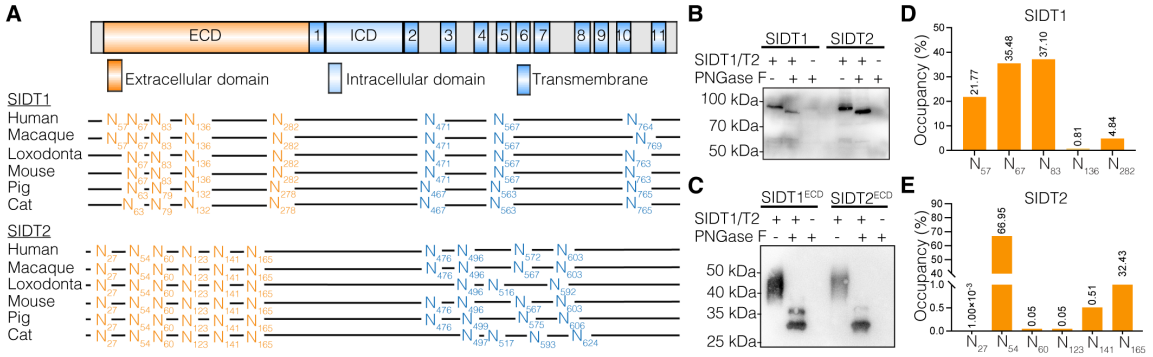

Figure 1. The mammalian SID-1 transmembrane family is *N*-glycosylated. A Domain schematic of human SIDT1 (upper panel) and conservation of *N*-glycosylation sites in mammalian SIDT1 and SIDT2 based on sequence alignment (bottom panel). **B** De-*N*-glycosylation analysis of full-length SIDT1 and SIDT2 with (+)/without (-) PNGase F, analyzed using Western blot with anti-Flag antibody. **C** De-*N*-glycosylation analysis of SIDT1^{ECD} and SIDT2^{ECD} with (+)/without (-) PNGase F, analyzed using Western blot with anti-His antibody. **D, E** Quantification of the abundance of glycopeptides at each glycosylation site of SIDT1 (**D**) and SIDT2 (**E**) through high-resolution LC-MS/MS analysis.

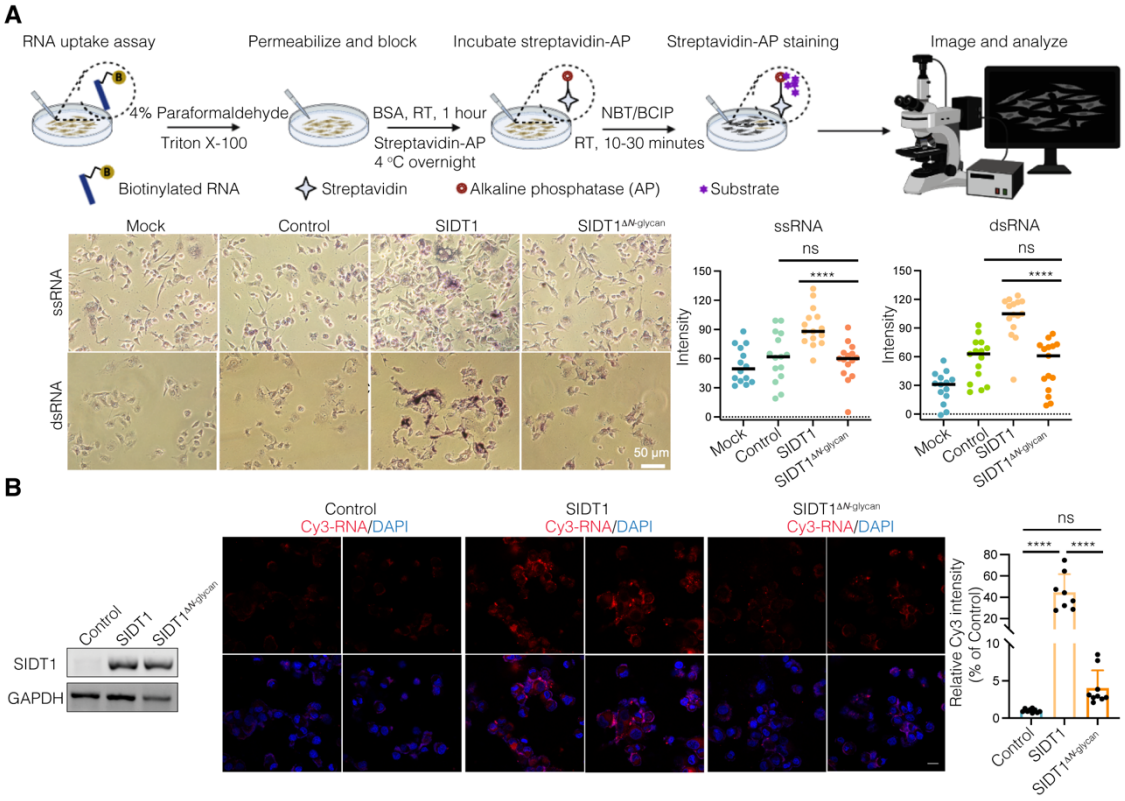

Figure 2. *N*-glycosylation is required for SIDT1-mediated RNA uptake. A Schematic diagram of the SIDT1-mediated RNA uptake by streptavidin-AP staining (upper panel). Representative images of streptavidin-AP staining of SIDT1 or SIDT1$^{\Delta N\text{-glycan}}$ transfected HEK293T cells after the uptake of synthetic biotinylated ssRNA or dsRNA, and the statistical analyses are shown (right panel). Scale bar, 50 μm. The statistical significance is determined by One-way ANOVA. ns, not significant, ****P < 0.0001. **B** Uptake of Cy3-labeled dsRNA by wild-type SIDT1 or SIDT1$^{\Delta N\text{-glycan}}$ transfected PANC1 cells at pH 7.5 were imaged by fluorescence (middle panel) and expression of SIDT1 was detected by Western blot (left panel). Images processed with ImageJ, and the statistical analyses are shown (right panel). Scale bar, 20 μm. One-way ANOVA. ns, not significant, **P < 0.01.

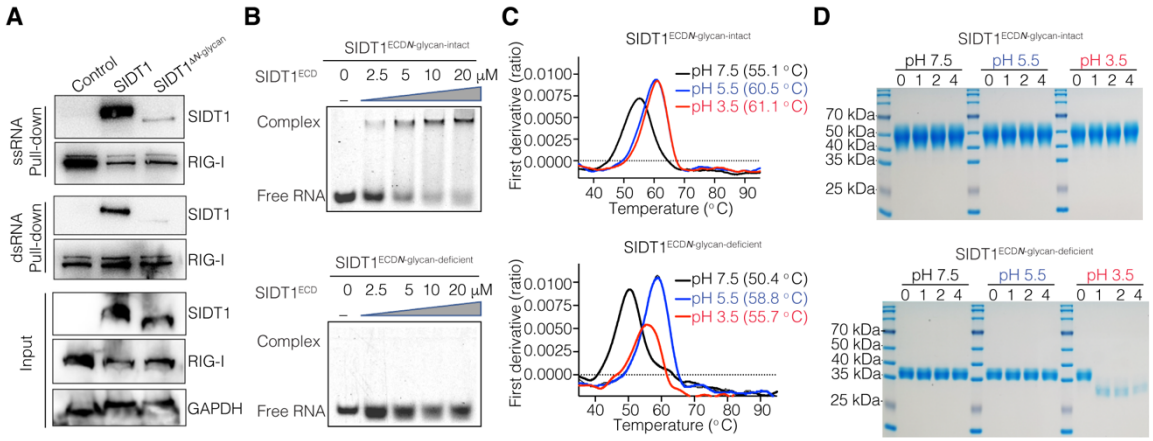

Figure 3. Effect of *N*-glycosylation on RNA binding and protein stability of SIDT1. A RNA pull-down assays with proteins were conducted using extracts from HEK293T cells transfected with wild-type SIDT1 or SIDT1$^{\Delta N\text{-glycan}}$ variant. Western blot was analyzed for wild-type SIDT1 and SIDT1$^{\Delta N\text{-glycan}}$ (Flag tag). Representative results from ⩾ 3 independent pull-down assays are shown. HEK293T cells transfected with RIG-I were used as positive controls. **B** RNA binding of SIDT1$^{\text{ECD}N\text{-glycan-intact}}$ or SIDT1$^{\text{ECD}N\text{-glycan-deficient}}$ as determined by EMSA. The final protein concentrations of SIDT1$^{\text{ECD}N\text{-glycan-intact}}$ or SIDT1$^{\text{ECD}N\text{-glycan-deficient}}$ in lanes 1-5 are 0, 2.5, 5, 10, and 20 μM, respectively, and the final 5'-FAM-labeled ssRNA concentration is 2.5 μM. Complex: bound; Free ssRNA: unbound. **C** Protein stability of SIDT1$^{\text{ECD}N\text{-glycan-intact}}$ and SIDT1$^{\text{ECD}N\text{-glycan-deficient}}$ was recorded in real time as the temperature increased from 35 to 95 °C. DSF profiles (ratio between fluorescence at 350 nm and 330 nm) are shown. **D** Time-chase experiments show the degradation of SIDT1$^{\text{ECD}N\text{-glycan-intact}}$ and SIDT1$^{\text{ECD}N\text{-glycan-deficient}}$ at different pH values (pH 7.5, 5.5, and 3.5; analyzed by SDS-PAGE) and incubation for the experimental period of 0/1/2/4 hours. Representative results from ⩾3 independent experiments are shown.

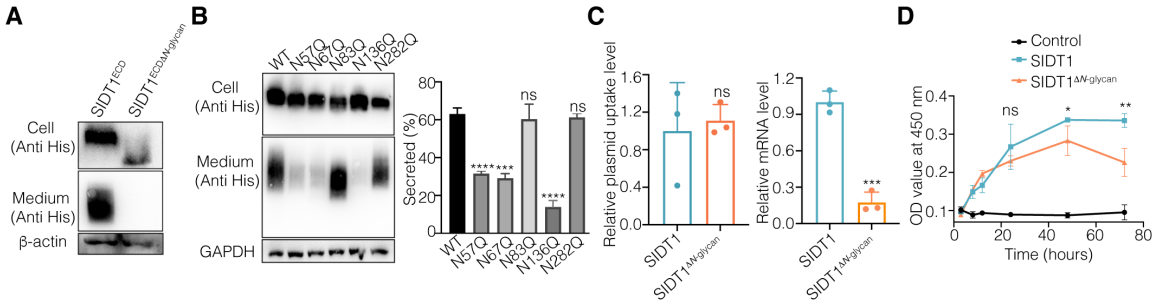

Figure 4. *N*-glycosylation is required for proper folding of SIDT1. A The effect of *N*-glycosylation on the secretion of wild-type SIDT1^{ECD} and SIDT1$^{ECD\Delta N\text{-glycan}}$ (cell and medium), and protein levels were analyzed by Western blot. **B** Secretion of the wild-type (WT), N57Q, N67Q, N83Q, N136Q and N282Q SIDT1^{ECD} variants was analyzed by Western blot. Band density was quantified using ImageJ software (right panel). Data are expressed as means ± SD, and values labeled with different letters are significantly different. Statistical significance is determined by One-way ANOVA. ns, not significant, ***P < 0.001, ****P < 0.0001. **C** The relative plasmid uptake (left panel) and mRNA expression levels (right panel) of SIDT1 and SIDT1$^{\Delta N\text{-glycan}}$ in HEK293T cells were examined by RT-PCR and normalized against GAPDH. mRNA data are expressed as means ± SD, and values marked with different letters are significantly different. Statistical significance is determined by two-tailed Student's *t*-test, ***P < 0.001. **D** Time-course experiments for protein levels of SIDT1 and SIDT1$^{\Delta N\text{-glycan}}$ were measured by ELISA. Statistical significance is determined by ANOVA. ns, not significant, **P < 0.01, *P < 0.05.

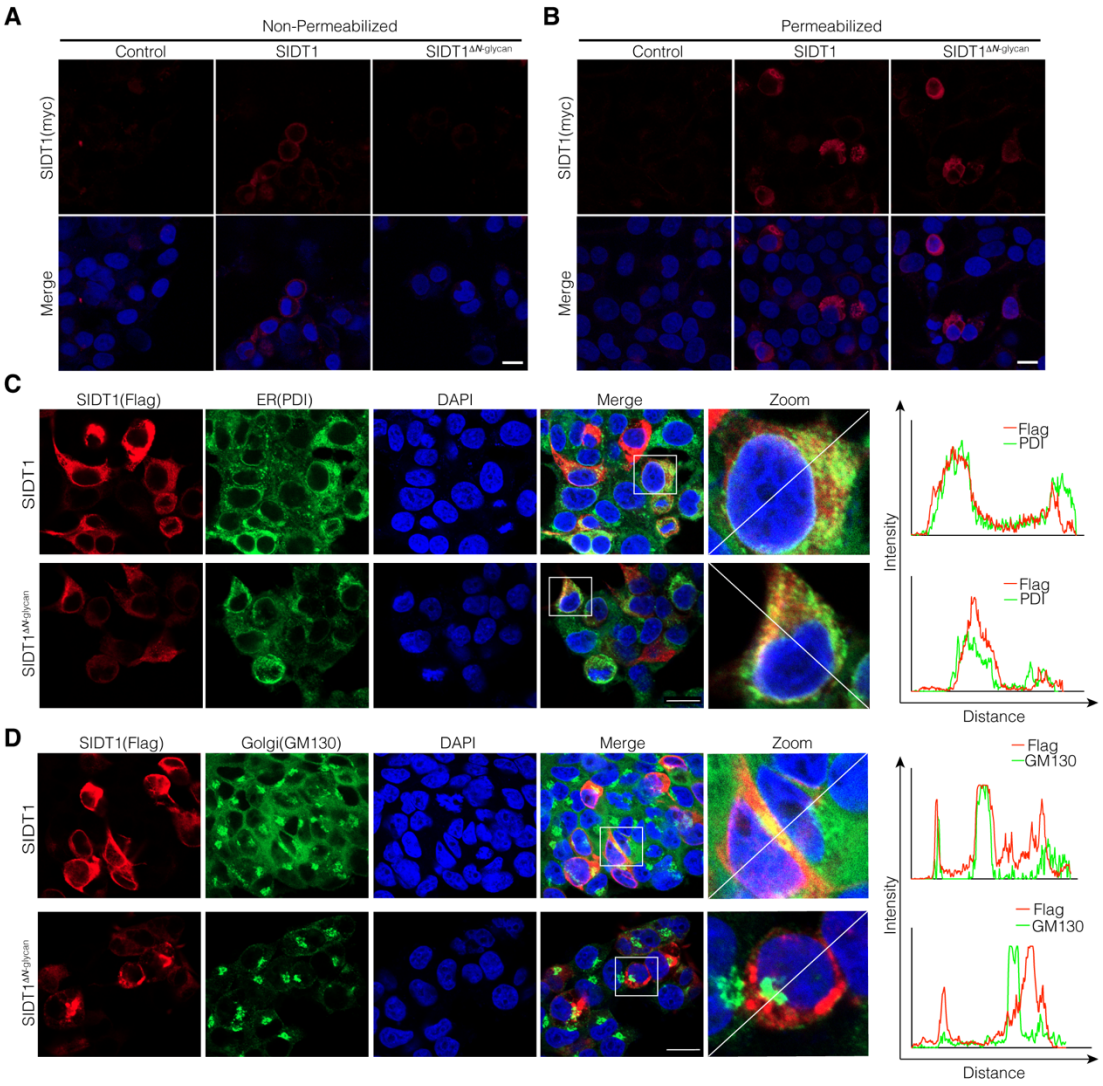

Figure 5. *N*-glycosylation is important for intracellular trafficking and cell surface expression of SIDT1. A, B Cell surface expression of wild-type SIDT1 and SIDT1$^{\Delta N\text{-glycan}}$ variant was determined by indirect immunofluorescence in non-permeabilized (**A**) or permeabilized (**B**) HEK293T cells by probing with anti-myc antibody. DAPI (blue) was used for nuclear staining. Scale bar, 5 μm. **C** Representative confocal microscopy images showing the ER localization in cells expressing wild-type SIDT1 and SIDT1$^{\Delta N\text{-glycan}}$ variant. Anti-PDI (green) and anti-Flag (red) antibodies were used. Scale bar, 20 μm. **D**

Representative confocal microscopy images showing the Golgi localization in cells expressing wild-type SIDT1 and SIDT1$^{\Delta N\text{-glycan}}$ variant. Anti-MG130 (green) and anti-Flag (red) antibodies were used. Scale bar, 20 μm.